PCCP

Flow-driven instabilities in the Belousov–Zhabotinsky reaction: Modelling and experiments

R. Tóth,[a] A. Papp,[a] V. Gáspár,*[a] J. H. Merkin,[b] S. K. Scott[c] and A. F. Taylor[c]

[a] *Institute of Physical Chemistry, University of Debrecen, 4010 Debrecen, P.O. Box 7, Hungary*
[b] *Department of Applied Mathematics, University of Leeds, Leeds, UK LS2 9JT*
[c] *School of Chemistry, University of Leeds, Leeds, UK LS2 9JT*

Received 22nd November 2000, Accepted 18th January 2001
First published as an Advance Article on the web 26th February 2001

The development of propagating patterns arising from the differential flow of reactants through a tubular reactor is investigated. The results from a series of experimental runs, using the BZ reaction, are presented to show how the wavelength and propagation speed of the patterns depend on the imposed flow velocity and the concentration of BrO_3^- in the inflow. A model for this system, based on a two-variable Oregonator model for the BZ reaction, is considered. A stability analysis of the model indicates that the mechanism for pattern formation is through a convective instability. Numerical simulations confirm the existence of propagating patterns and are in reasonable agreement with the experimental observations.

1 Introduction

An important feature of spatially distributed chemical systems is their ability to support spatio-temporal structures. The original idea for structure generation, proposed by Turing,[1] is that, if the diffusion coefficients of the reacting species in a system with feedback kinetics are sufficiently different, this can destabilize the spatially uniform steady state to produce steady waves (or patterns) in the reactant concentrations. This basic idea has been tested theoretically on a series of prototype model schemes, though it is only relatively recently that Turing patterns have been observed experimentally.[2–4] The realization that spatial structures could be generated experimentally in chemical systems provided a strong impetus to the development of new reactors for observing such phenomena, see ref. 5 for a recent review.

One recent development is the differential-flow reactor, devised originally by Rovinsky and Menzinger.[6–9] The basic idea behind this reactor is that the reacting species flow through it at different rates. This differential transport can initiate instabilities in the basic state leading to propagating wave packets of reactant concentrations, moving in the direction of the flow. In the original experiments, and in the ones described below, the BZ system is used with the differential flow being produced by immobilizing the ferroin on cation-exchange beads while the other reactants flow through the reactor at a rate controlled by an applied pressure difference.

The convective nature of this instability, termed the differential-flow induced chemical instability or DIFICI, was recognised in computer simulations[9] and in theoretical studies using Brusselator[10] and Gray–Scott[11,12] kinetics. These theoretical studies have been extended to include cases where all the reactants flow (or migrate), though at different rates, through the reactor.[13,14] This additional effect arises from the application of a (constant) electric field, under which ionic species migrate at a rate proportional to their diffusion coefficient. In these cases, interactions of DIFICI with Turing and Hopf bifurcations are possible, resulting in a wide range of complex spatio-temporal behaviour including the possibility of spatio-temporal chaos.

Here we reconsider the DIFICI experiments with a view to obtaining a more quantitative description of the underlying mechanism. To this end we have performed a series of experimental runs for different flow rates and for different bromate concentrations in the feed. In each case, the propagation velocity and wavelength of the resulting patterns were measured and their dependence on the flow velocity established. We have also considered a model for the system based on a two-variable Oregonator scheme for the BZ reaction. A stability analysis of this model predicts parameter ranges where the convective instability driving the DIFICI can be found. This information was then used to determine parameter values suitable for numerical simulations. These show the development of a series of propagating wave forms arising from a single initial perturbation to the basic state. Our theoretical considerations reveal that these propagating waves originate from a somewhat different mechanism to the patterns (steady and propagating) seen in other types of flow reactors.[15]

The theory is derived in terms of the flow velocity of reactants within the reactor. To be able to use the results from our model to interpret the experimental findings, this velocity needs to be determined from the measured flow rates used in the experiments. This requires further calculations to estimate the packing density and void fraction of the cation-exchange beads in the tubular reactor. This aspect has not been addressed before for this particular set up.

2 Experiments

2.1 Experimental setup

The experiments were run in a tubular reactor (Fig. 1) similar to that developed by Rovinsky and Menzinger.[6,7] The tube was packed with DOWEX 50 × 4–400 cation-exchange resin on which ferroin was immobilized. Before loading with ferroin, the ion exchanger was washed 5–7 times with distilled water. Each time, after the main part of the beads had settled, the liquid fraction was decanted; the remaining suspension of the resin in water was then transferred into a measuring cylinder. When the beads had settled in the measuring cylinder, the volume they occupied was determined. This volume (note that this is still a suspension) was chosen as the reference value for the loading with ferroin. The concentration of ferroin on the resin calculated in this way was 1×10^{-3} M. However,

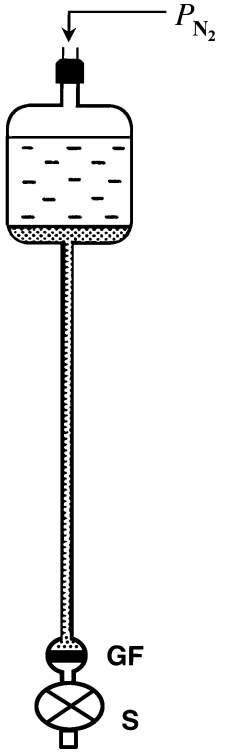

Fig. 1 Schematic representation of the experimental apparatus. The internal diameter and length of the tube are 5.0 mm and 29 cm respectively. GF is a G3 glass frit, S is a stopcock, *P* indicates the imposed pressure of nitrogen used to drive the fluid flow. This pressure is controlled by a standard gas regulator. (Figure adapted from ref. 7.)

assuming that the free volume occupied by the flowing solution is about a third of the total volume (see later) the ferroin concentration in the free solution is 3×10^{-3} M. The loaded beads were mixed with some water and transferred to the tubular reactor by applying a small excess of pressure. The beads needed 3–4 h to settle in the tube then catalyst-free BZ solution was poured into the top reservoir of the reactor. The concentrations in the reacting BZ mixture were: [BrMA] = 0.4 mol dm^{-3}, [H_2SO_4] = 0.02 + 0.4 mol dm^{-3} from the stock solution of bromomalonic acid (BrMA), [BrO_3^-] was varied in the experiments (0.6, 0.8 and 0.95 mol dm^{-3}).

Stock solution of bromomalonic acid. 0.4 mol dm^{-3} stock solution of BrMA was prepared according to the recipe given by Zaikin and Zhabotinsky.[16] 10.41 g of malonic acid was dissolved in a mixture of 33.3 cm^3 of 2 mol dm^{-3} NaBr solution, 25 cm^3 of 4 mol dm^{-3} H_2SO_4 solution and 20.87 cm^3 distilled water in a three-neck flask supplemented by a thermometer, a reflux condenser and a dropper funnel. The mixture was stirred with a magnetic stirrer and cooled to 10 °C with ice from outside the flask. With the temperature carefully maintained at 10 °C, 20.83 cm^3 of 1.6 mol dm^{-3} $NaBrO_3$ solution was added to the mixture drop by drop from the funnel. Because of the reaction between acidic bromate and bromide ions the mixture turns to yellow at each drop, hence time was allowed for the colour to disappear before the next drop was added. This ensures a slow bromination process without losing bromine to the gas phase.

Generating wave patterns. The volumetric flow rate of the BZ mixture inside the tubular reactor Q was controlled by applying compressed nitrogen gas, Q was assumed proportional to the gas pressure. The value of Q was checked frequently by measuring the time for collecting 5.0 ml solution at the bottom of the tube. The experiment was started when the flow rate became stabilized. In the absence of flow, the beads in the tube were red (reduced state) without definite pattern formation indicating that the effect of gravity is negligible. When gas pressure was applied, pale blue (oxidation) waves appeared and propagated down the tube.

Measurements of wave velocity. The wave patterns were recorded on videotape and the images processed on a PC. ImageJ and Optimas programs were used to determine the velocity of the DIFICI waves, c_w, by measuring the time a wave had travelled a known distance down the tube. The wavelength, λ, was determined by measuring the distance between the fronts of two consecutive waves.

The velocity of the waves was measured as a function of the applied gas pressure. Since there is a slight variation in the packing density of the resin in the tube and the velocity of the waves varied within a small range even at the same gas pressure, there is a need to convert the applied pressure to the actual flow velocity c_f inside the tube. This involved the measurement of the volumetric flow rate.

Calibration. The flow velocity is defined by

$$c_f = \frac{Q}{A} \tag{1}$$

where A is the 'free surface area' within the tube. The free surface area can be calculated from

$$A = \frac{V_0}{L} \tag{2}$$

where V_0 is the 'free volume' within the tube and L is its length. The free volume is defined as

$$V_0 = V - V_b = \pi r^2 L - V_b \tag{3}$$

where V is the total volume of the tube, V_b is the volume occupied by the beads and r is the radius of the tube.

The free volume was determined experimentally in two ways. (1) A known volume of water was placed in a measuring cylinder and a known amount of the dry resin added to it. The change in total volume was recorded. The free volume is then the difference between the volume the settled resin occupied and the measured change in volume. (2) The unloaded resin was mixed with some water and the suspension was transferred to the tubular reactor. The water in the reservoir was drained off until level with the top of the resin. A 0.1 mol dm^{-3} solution of NaBr was then carefully put into the reservoir. A Petri dish containing 10 cm^3 of 0.1 mol dm^{-3} $AgNO_3$ solution was placed under the tube. After opening the stopcock and applying some extra pressure, the volume change until the first drop of brown precipitate appeared in the $AgNO_3$ solution was measured. With both methods, the free volume was found to be about 31–34% of the total volume.

2.2 Results

Examples of DIFICI waves are illustrated in Fig. 2. Successive images, taken at 2.8 s intervals, are shown from left to right for a 7.7 cm section of the tube. Blue oxidation waves are seen propagating downward through this section with a velocity $c_w = 0.167$ cm s^{-1} and with a mean wavelength of 2.1 cm. Note that the acidity was increased for this particular experiment to enhance the colour contrast. A lower concentration was used for the experiments reported in later figures. The dark areas at the top of the field of vision correspond to more densely-packed sections of the tube.

The variation of the experimentally-observed wave velocity is shown in Fig. 3. This diagram is distinguished from that in previous work[6] as the wave velocity is plotted against the actual flow velocity c_f of the fluid along the DIFICI reactor rather than as a function of the driving pressure. The response

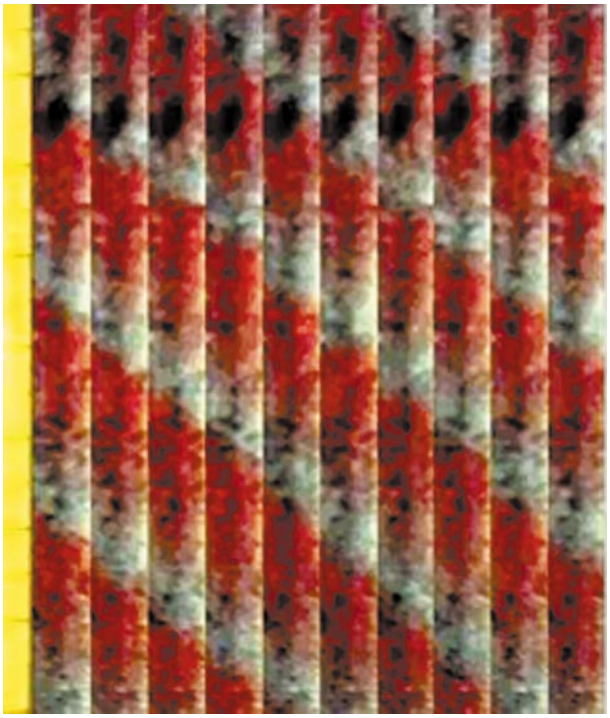

Fig. 2 Experimental images of DIFICI waves at $c_f = 0.138$ cm s^{-1}. Successive images, taken at 2.8 s intervals, are shown from left to right for a 7.7 cm section of the tube. Blue oxidation waves are seen propagating downward through this section with a velocity $c_w = 0.167$ cm s^{-1} and with a mean wavelength of 2.1 cm.

is linear, with the gradient of the fitted straight line varying most weakly with the bromate ion concentration—linear regression gave the following gradients: 1.04 ($\pm$0.05), 0.90 ($\pm$0.08) and 0.83 ($\pm$0.12) for $[BrO_3^-]_0 = 0.6$, 0.8 and 0.95 M respectively. The intercepts could not be resolved from the uncertainty sufficiently to determine any trend, although in general terms, the higher the bromate ion concentration, the lower the wave speed for a given flow velocity. In the absence of flow, no pattern was observed: we were unable to determine any "critical" flow velocity experimentally as patterns were observed even for the lowest non-zero flow (approximately 0.03 cm s^{-1}) attainable.

The wavelength λ of the DIFICI wave was measured in our experiments and is typically of the order of a few centimetres. Small variations in the distance separating oxidation fronts were observed in a particular experimental run. The mean wavelength λ was calculated by averaging over a sequence of waves. The variation of λ with the flow velocity for different

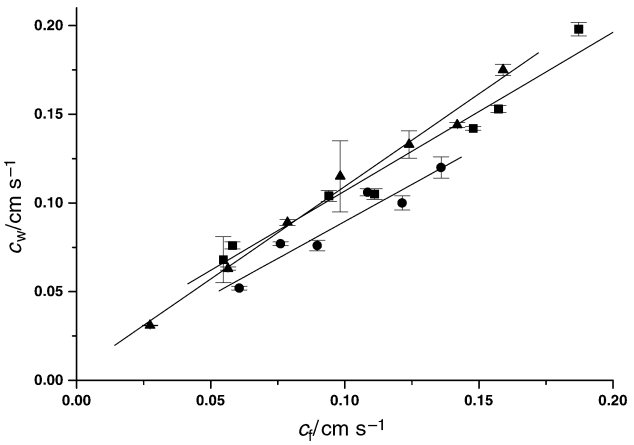

Fig. 3 Velocity of the DIFICI waves c_w plotted against flow velocity c_f; $[BrO_3^-] = 0.6$ (▲), 0.8 (■), 0.95 (●) mol dm^{-3}.

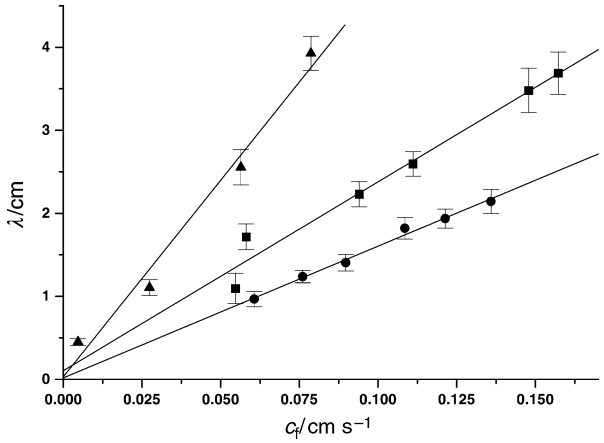

Fig. 4 Wavelength λ plotted against the flow velocity c_f. Concentrations of $[BrO_3^-]$ are as in Fig. 2.

bromate concentrations was determined and is shown in Fig. 4. Again, a reasonable linear relationship is observed. A systematic trend in the gradient in terms of the bromate ion concentration emerges, with the gradient g increasing as the concentration decreases: $g = 15.9$ ($\pm$0.8), 22.8 ($\pm$2.0) and 47.3 ($\pm$4.7) s for $[BrO_3^-]_0 = 0.95$, 0.8 and 0.6 M respectively. A log–log plot for the three data sets suggests that the gradient is proportional to $[BrO_3^-]_0^{-2.4(\pm 0.1)}$. The intercepts in Fig. 4 are not statistically significantly different from zero.

3 Model

The analysis and numerical simulations are based on the Field–Kőrös–Noyes model[17] of the BZ reaction through a spatially varying, two-species Oregonator model,[18] in which the reactants considered are $X \equiv HBrO_2$ and $Z \equiv M_{ox}$ (the oxidized form of the catalyst). This model can be represented schematically as (see ref. 19, for example)

$$\begin{aligned} A + Y &\rightarrow X + P; & \text{rate} &= k_3[A][Y] \\ X + Y &\rightarrow 2P; & \text{rate} &= k_2[X][Y] \\ A + X &\rightarrow 2X + 2Z; & \text{rate} &= k_5[A][X] \\ 2X &\rightarrow A + P; & \text{rate} &= k_4[X]^2 \\ B + Z &\rightarrow \tfrac{1}{2}fY; & \text{rate} &= k_c[B][Z] \end{aligned} \quad (4)$$

$A \equiv BrO_3^-$ and B (all the oxidizable organic species) are assumed to have constant concentrations throughout, $P \equiv HOBr$ is a product of the reaction and $Y \equiv Br^-$ is taken to be in the quasi-steady state, so that

$$[Y] = \frac{\frac{1}{2}fk_c[B][Z]}{k_3[A] + k_2[X]} \quad (5)$$

The model is augmented to include a convective term to represent the flow of $HBrO_2$ at a constant velocity c_f through the reactor; M_{ox} is assumed to be immobile. This leads, using the standard Tyson–Fife scalings,[20–22] to the dimensionless equations for our model as

$$\varepsilon \frac{\partial u}{\partial t} = \frac{\partial^2 u}{\partial x^2} - \phi \frac{\partial u}{\partial x} + u(1-u) - \frac{fw(u-q)}{(u+q)} \quad (6)$$

$$\frac{\partial w}{\partial t} = u - w \quad (7)$$

on $0 < x < \infty$, $t > 0$, where x and t are dimensionless space and time variables and where u and w are the (dimensionless) concentrations of X ($HBrO_2$) and Z (M_{ox}) respectively, with

$$[X] = \frac{k_5[A]}{2k_4}u, \quad [Z] = \frac{(k_5[A])^2}{k_c k_4[B]}w$$

f is the stoichiometric factor, and

$$\varepsilon = \frac{k_c B}{k_5 A} \quad \text{and} \quad q = \frac{2k_3 k_4}{k_2 k_5}$$

are the usual parameters for the Oregonator model (see ref. 19, for example). ϕ is the dimensionless flow velocity, related to its dimensional value c_f by

$$c_f = (Dk_5 A)^{1/2}\phi \tag{8}$$

where D is the diffusion coefficient for $HBrO_2$. Note that eqn. (6) and (7) have been rendered dimensionless using $(D/k_5 A)^{1/2}$ and $(k_c B)^{-1}$ as length and time scales respectively.

Initially the system (6) and (7) is at the stable, spatially uniform steady state, with

$$u = w = u_s = \tfrac{1}{2}(1 - (f+q) + \sqrt{(1-f-q)^2 + 4q(1+f)}) \tag{9}$$

for all x. For the numerical simulations zero-flux boundary conditions are applied at $x = 0$ (inlet) as well as at large distances along the reactor (formally as $x \to \infty$).

We consider a situation for which, in the absence of flow (and diffusion), the steady state is stable to small perturbations. We then wish to determine the conditions under which the differential flow, represented by the flow parameter ϕ, can lead to instabilities arising from these small perturbations. To do so we consider a linear stability analysis.

3.1 Linear stability analysis

We linearize eqn. (6) and (7) about the steady state, eqn. (9), writing

$$u = u_s + U, \quad w = u_s + W, \quad U, W \text{ small}$$

with eqn. (6) and (7) becoming

$$\varepsilon \frac{\partial U}{\partial t} = \frac{\partial^2 U}{\partial x^2} - \phi \frac{\partial U}{\partial x} + \alpha U - \beta W$$

$$\frac{\partial W}{\partial t} = U - W \tag{10}$$

where

$$\alpha = 1 - 2u_s - \frac{2qfu_s}{(u_s+q)^2}, \quad \beta = \frac{f(u_s - q)}{(u_s + q)} \tag{11}$$

Note that $\beta > 0$ for all reasonable values of the model parameters. For our theoretical discussion it is convenient to extend the spatial domain to $-\infty < x < \infty$ and to assume that a single perturbation, localized to $x = 0$, is made at $t = 0$.

Our basic assumption about the stability of the system in the absence of flow (and diffusion) requires

$$T_r = \alpha - \varepsilon < 0, \quad \Delta = \beta - \alpha > 0 \tag{12}$$

We look for a solution of the linear eqn. (10) in terms of Fourier transforms, namely

$$(U, W) = \frac{1}{2\pi}\int_{-\infty}^{\infty} (\bar{U}_0(k), \bar{W}_0(k))\exp(\omega(k)t + ikx)\, dk \tag{13}$$

where ω satisfies the dispersion relation

$$\varepsilon\omega^2 + (k^2 + i\phi k - T_r)\omega + \Delta + (k^2 + i\phi k) = 0 \tag{14}$$

T_r and Δ are given by eqn. (12). $\bar{U}_0$ and $\bar{W}_0$ are the Fourier transforms of the initial (small) perturbation and, for perturbations with compact support, are analytic functions in the complex k-plane. Eqn. (14) shows that diffusion alone cannot destabilise the system, for, with $\phi = 0$ and conditions (12) satisfied, $\mathrm{Re}(\omega) < 0$ for all wavenumbers k. This may not be the case when $\phi > 0$ and to investigate this possibility we first obtain the neutral curve, *i.e.*, the curve in the ϕ–k^2 parameter space on which $\mathrm{Re}(\omega) = 0$. From dispersion relation (14) we find that this is given by

$$\phi^2 = \frac{(\Delta + k^2)(k^2 - T_r)^2}{k^2(\alpha - k^2)} \tag{15}$$

Expression (15) needs the extra condition that $\alpha > 0$, with eqn. (15) then defined on $0 < k^2 < \alpha$. The neutral curves, as given by eqn. (15), have vertical asymptotes at $k^2 = 0$ and $k^2 = \alpha$, and are positive on $0 < k^2 < \alpha$. It is easily shown that they have a single local minimum on this range, with a typical case being shown in Fig. 5. The main point to note from eqn. (15), illustrated by Fig. 5, is that there is a minimum value ϕ_{min} for ϕ (where $\phi_{min} > 0$) such that, when $\phi > \phi_{min}$, there is a range of wavenumbers k over which $\mathrm{Re}(\omega) > 0$. Hence the system is unstable to general small perturbations for all $\phi > \phi_{min}$.

To determine the nature of this instability, we need to obtain the asymptotic behaviour of the Fourier integrals (13) for t large and x fixed. We use the method of steepest descent[23] which shows that the dominant terms arise from the saddle-point (k_s, ω_s) in the complex k-plane [where $(d\omega/dk) = 0$]. This is given by, from eqn. (14), $k_s = -(i\phi/2)$ and then

$$\varepsilon\omega_s^2 + \left(\frac{\phi^2}{4} - T_r\right)\omega_s + \left(\Delta + \frac{\phi^2}{4}\right) = 0 \tag{16}$$

From eqn. (16), $\mathrm{Re}(\omega_s) < 0$ for all ϕ when conditions (12) apply and hence any perturbation will die away for t large and x fixed. However, the fact that, for $\phi > \phi_{min}$, there is a range of wavenumbers over which $\mathrm{Re}(\omega) > 0$ implies that the system is convectively unstable, following the general treatment (based on CGL equations) given by Deissler.[24,25] This means that there is a moving reference frame in which any (small) perturbation will grow (equilibration at finite amplitude through nonlinear effects may be expected). Thus we expect that any small perturbation will grow to produce a finite disturbance to the system. This will propagate through the system which will then return to its original spatially uniform state.

Hence, we have determined the conditions for convective instability as, using eqn. (11) and (12),

$$0 < \alpha < \varepsilon, \quad \phi > \phi_{min} \tag{17}$$

From eqn. (11), α depends only on q and f (and not on ε) and a typical plot of α against f is shown in Fig. 6a (here for $q = 0.002$). The graph crosses the axis at two points f_{C_1} and f_{C_2}, one when the system is in the oxidized state, f_{C_1}, and one when it is in its reduced state, f_{C_2}, in this example $f_{C_1} = 0.5061$, $f_{C_2} = 2.3943$. The line $\alpha = \varepsilon$ (where the spatially uniform system undergoes a Hopf bifurcation) is parallel to the axis

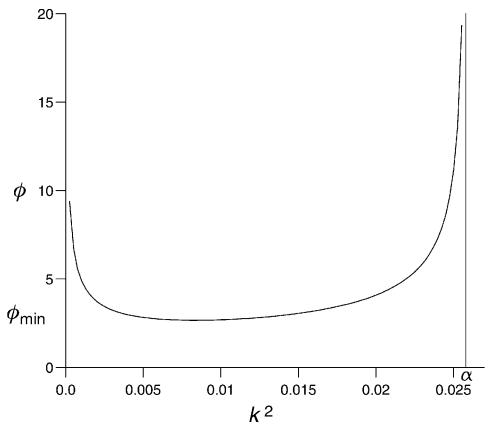

Fig. 5 A typical neutral curve eqn. (15), the curve in the ϕ–k^2 parameter plane on which $\mathrm{Re}(\omega) = 0$ (ω given by the dispersion relation eqn. (14)). The parameter values used for this figure are $q = 0.002$, $\varepsilon = 0.05$, $f = 2.35$ ($\alpha = 0.025\,79$) and has $\phi_{min} = 2.6670$.

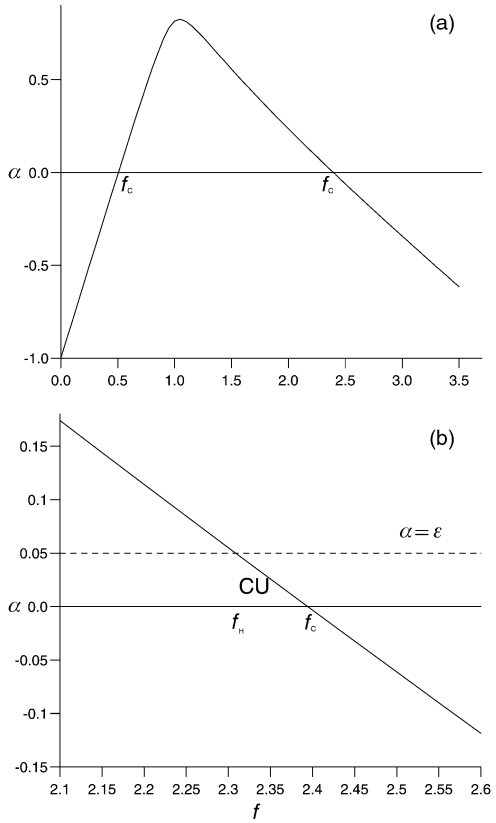

Fig. 6 (a) A graph of α against f for $q = 0.002$. The points, labelled f_C, where the graph crosses the axis show the onset of convective instability. (b) The region where the system is convectively unstable (labelled CU) between where the curve crosses the axis and the line $\alpha = \varepsilon$.

and cuts the curve at two points, f_{H_1} and f_{H_2} (for $\varepsilon = 0.05$ these are at $f_{H_1} = 0.5317$ and $f_{H_2} = 2.3087$). It is in the range of f between f_{C_i} and f_{H_i} ($i = 1, 2$) that the system is convectively unstable, provided $\phi > \phi_{min}$. This is illustrated in Fig. 6b for the system in its reduced state, the region of possible convective instability is labelled CU in the figure.

There are two features to note especially about Fig. 6a. First, it predicts that convective instabilities can occur in both the reduced state (larger f and lower values of u_s) and the oxidized state (lower f and higher values of u_s). Perhaps more importantly, it predicts that there is only a relatively narrow 'window', just beyond where oscillations will be seen in the batch system, where convective instabilities can occur. This 'window' decreases as ε decreases (*i.e.* the system becomes more excitable). Thus, for fixed values of the other parameters, as f is increased (for the reduced state) from its Hopf bifurcation value f_H (at $\alpha = \varepsilon$) to $f = f_C$ (at $\alpha = 0$) the system can sustain convective instabilities for flow velocities above the critical ϕ_{min}. Note that ϕ_{min} depends on all the kinetic parameters. For $f > f_C$ the system is stable for all ϕ. A graph of the corresponding values of ϕ_{min} is shown in Fig. 7 (for $q = 0.002$, $\varepsilon = 0.05$). Note that $\phi_{min} \to 0$ as $f \to f_H$ and $\phi_{min} \to \infty$ as $f \to f_C$, as expected from eqn. (15).

For $f > 1$ approximate expressions for f_C and f_H can be obtained by exploiting the result that $u_s \simeq q(f + 1)/(f - 1)$ for $q \ll 1$.[26] This gives

$$f_C = \sqrt{2} + 1 + O(q),$$
$$f_H = (1 - \varepsilon) + \sqrt{2 - 2\varepsilon + \varepsilon^2} + O(q)$$
$$\simeq (\sqrt{2} + 1) - \varepsilon\left(1 + \frac{\sqrt{2}}{2}\right) \quad (18)$$

for q (and ε) small.

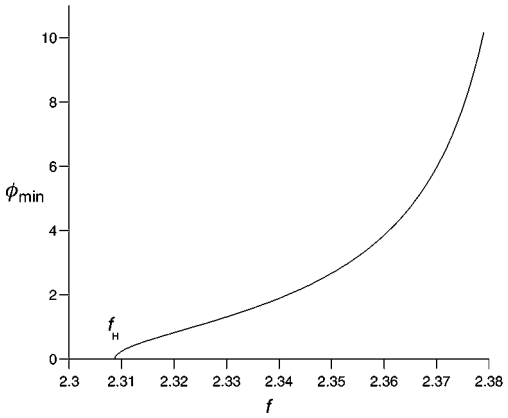

Fig. 7 ϕ_{min} plotted against f for the reduced state ($q = 0.002$, $\varepsilon = 0.05$).

3.2 Numerical simulations

Eqn. (6) and (7) were solved numerically using a standard implicit algorithm, based on the Crank–Nicolson scheme, for integrating parabolic systems. Newton–Raphson iteration was used to solve the sets of nonlinear finite-difference equations which arise at each time step. The spatial domain consisted of 12 000 grid points with a mesh size $\Delta x = 0.1$ being used. An adjustable time-step procedure was used to maintain overall accuracy, typically $\Delta t = 0.016$. The integrations were started with the system in its spatially uniform configuration perturbed initially by increasing slightly the value of u over the first 10 grid points. No further perturbations were made during the course of the integrations and zero-flux boundary conditions were applied at both ends of the computational domain.

To illustrate the development of convective instabilities we took $\varepsilon = 0.05$, $q = 0.002$ and $f = 2.32$, for these parameter values $\phi_{min} = 0.822$. Results for $\phi = 1.5$ are shown in Fig. 8. In Fig. 8a and b we give profile plots of u and w, the dimensionless concentrations of $HBrO_2$ and M_{ox} respectively, and in Fig. 8c we plot the position x_f of the 'pulses' in u that develop; in this figure the lines represent the position of the front of the pulse (where u first takes the value $u = 0.1$).

The perturbation applied at $t = 0$ generates an initial wave, this would be seen without the flow though its speed c is higher ($c = 60.8$ for $\phi = 1.5$ whereas $c = 29.9$ when $\phi = 0$). This first wave propagates through the system and, when this has recovered sufficiently, a second wave develops. This starts downstream of where the initial perturbation was applied (second wave in Fig. 8c). Fig. 8a(i) and b(i) ($t = 7.98$) are plotted when the second wave has just formed. There is evidence of a further small perturbation behind this second wave. This dies out in the refractory tail of the second wave as it propagates. The w profile has a pulse-like form in Fig. 8b(i). This spreads to a profile similar to the first wave through the rear part remaining fixed and the front part propagating forwards. Initially the second wave has a slightly higher speed than the first wave.

By $t = 16.39$ (Fig. 8a(ii) and b(ii)) the second wave has propagated further along the computational domain and a third wave has just formed, downstream of where the second wave was initiated. A further small perturbation can be seen at the rear of the third wave as it develops. This grows to form a fourth wave (Fig. 8a(iii) and b(iii), $t = 17.35$). The third wave then propagates forwards, initially with a speed slightly higher than the first two waves. The fourth wave forms close behind the third wave and moves only slowly to start with. The effect of the refractory tail of the third wave is to reduce the amplitude of the fourth wave from its initial development and, as the two waves become more separated, this grows again to form a fully developed wave. The speed of the fourth wave

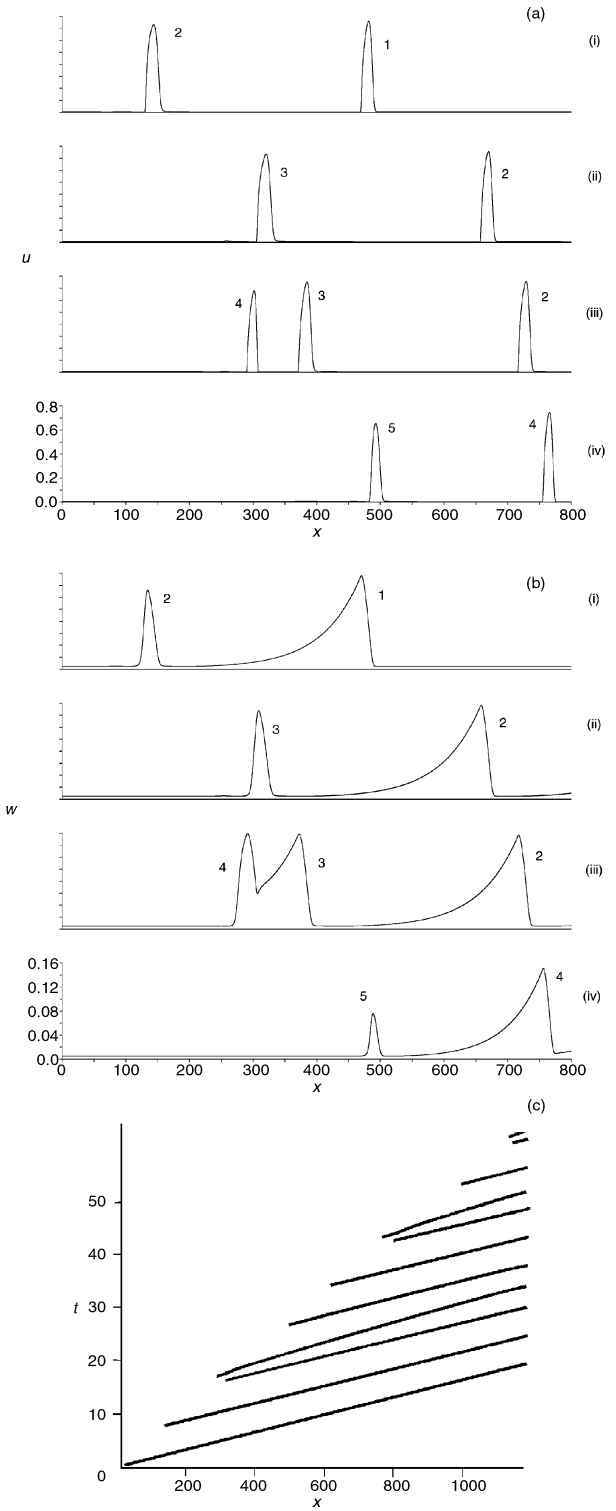

Fig. 8 Profile plots of (a) u and (b) w, the dimensionless concentrations of $HBrO_2$ and M_{ox} at $t = 7.98, 16.39, 17.35, 26.81$ to show the development of a convective instability. (c) the position x_f of the 'pulses' in u. The parameter values are $\varepsilon = 0.05$, $q = 0.002$, $f = 2.32$, $\phi = 1.5$.

increases as it becomes more separated from the third wave and a wave train is set up.

The next event is for a fifth wave to form after the fourth wave has propagated sufficiently far downstream. This is shown in Fig. 8a(iv) and b(iv) ($t = 26.81$) where the fifth wave has just formed. There is a perturbation behind this fifth wave but, unlike the previous case, this does not produce a wave and dies out as the fifth wave propagates. The speed of this fifth wave is comparable to speeds of the second and third

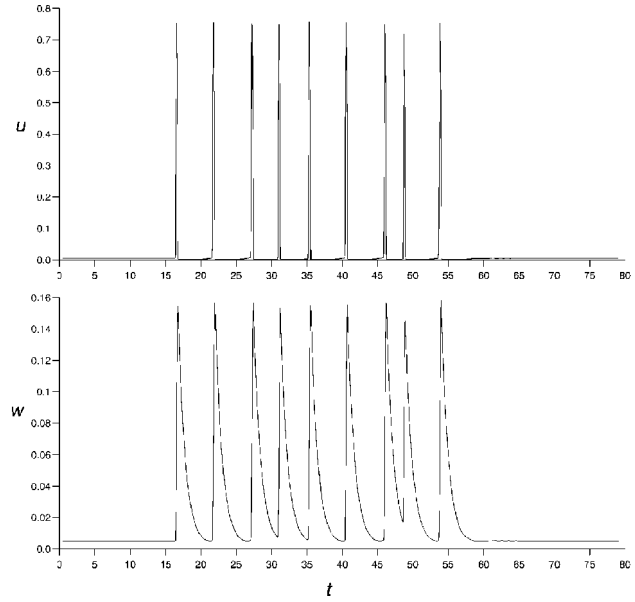

Fig. 9 The u and w time traces, plotted at $x = 1000$, to show the nature of the convective instability, arising from the single initial perturbation at $x = 0$, propagating through the system. The parameter values are $\varepsilon = 0.05$, $q = 0.002$, $f = 2.32$, $\phi = 1.5$.

waves. After the fifth wave has propagated a distance and the system has recovered sufficiently, another wave, the sixth, is generated in a manner analogous to the formation of the second wave (see Fig. 8c). This is initiated further downstream than where the fifth wave formed. After the sixth wave has developed, another pair of waves (seventh and eighth) are formed in a way analogous to the third and fourth waves (Fig. 8c). These are initiated still further downstream than the previous waves. As t increases further wave formation appears (Fig. 8c) with a total of 11 waves being seen in this computation, though the final pair of waves develop close to the end of the computational domain. No further wave formation was seen in this computation, though we can expect the scenario reported above to continue beyond the limits of our computational domain.

An important feature to note about this sequence of wave formation is that each successive wave is initiated further downstream than the previous ones (as can clearly be seen in Fig. 8c). The system then progressively returns to its original steady state ($u = w = u_s$) as the wave pattern propagates downstream. We illustrate this point by giving time traces of u and w at a given station. These are shown in Fig. 9 at $x = 1000$. This figure clearly shows that a considerable time elapses before the effect of the initial perturbation is felt. The system then undergoes several excursions from its initial state before returning to (and remaining at) this state. One final point to note is that, without a flow or with $\phi < \phi_{min}$, only a wave equivalent to the first wave shown in Fig. 8 is formed, no other wave development is seen.

4 Discussion

Our experiments have shown that a differential flow of reactants through a tubular reactor can lead to an instability in the basic state and to the propagating patterns reported previously.[6,7] This shows the reproducibility of this instability phenomenon. We have extended the previous studies by determining how the propagation speed and wavelength of the resulting patterns depends on the concentration of BrO_3^- in the feed and the flow velocity of the reactants. Further calibration of the reactor was required to determine this flow velocity in terms of the measured volumetric flow rate and the particle packing density.

We also considered a model for the reactor based on two-variable Oregonator kinetics for the BZ reaction. The results from our model show clearly the convective nature of the DIFICI instability, whereby an initial disturbance sets up a wave train that propagates through the reactor. Although the two-variable Oregonator kinetics that we use in the model are a very good paradigm for excitable systems, they have some deficiencies for direct quantitative comparison with experiments using the BZ reaction. However, we can try to obtain some estimates for the relation between model and experiments. To do so we need values for k_5, for which we take $k_5 = 42\ \mathrm{M}^{-2}\ \mathrm{s}^{-1}$,[19] D and the concentration of H^+. The experiments were performed with $[\mathrm{H}^+] \simeq 0.4$ M and for D we take $D = 2 \times 10^{-5}\ \mathrm{cm}^2\ \mathrm{s}^{-1}$. This latter value is appropriate for molecular diffusion, though in the model an 'effective' diffusion coefficient, which reflects the fact that the reactor can be thought of as a porous material, may be more realistic. With these values, and taking the mid value for $[\mathrm{A}] = 0.8$ M, we obtain the factors

$$\left(\frac{D}{k_5 A[\mathrm{H}^+]}\right)^{1/2} = 1.2 \times 10^{-3}\ \mathrm{cm},$$

$$(Dk_5 A[\mathrm{H}^+])^{1/2} = 1.6 \times 10^{-2}\ \mathrm{cm\ s}^{-1} \qquad (19)$$

for conversion between the dimensionless variables used in the model and their respective experimental values.

The parameter values used in the numerical simulations (Fig. 8 and 9) give $\phi_{\min} = 0.822$ which, from eqn. (19), corresponds to a critical velocity of $c_{\mathrm{f,\,crit}} \simeq 1.3 \times 10^{-2}\ \mathrm{cm\ s}^{-1}$ for the onset of pattern formation. If we take this as typical for the critical velocity, then it would be virtually impossible experimentally to distinguish between these velocities and no flow. This provides an explanation as to why no 'onset' effect was seen in the experiments. The value of ϕ used for Fig. 8 and 9 gives a velocity $c_{\mathrm{f}} \simeq 0.024\ \mathrm{cm\ s}^{-1}$, which corresponds to the lower end of the results presented in Fig. 3 and 4. The waves seen in the numerical simulation have a typical wavelength of 350 dimensionless units, corresponding, through eqn. (19), to $\lambda \simeq 0.42$ cm, which is consistent with this value of c_{f} in Fig. 4. To compare wave speeds we really need to take the value $\varepsilon c \simeq 3.0$ from theory, giving $c_{\mathrm{w}} \simeq 0.05\ \mathrm{cm\ s}^{-1}$, which is in reasonable agreement with the results shown in Fig. 3.

For 'excitability' in Oregonator kinetics the parameter ε should be small. In this case the model identifies that there is only a relatively narrow 'window' of parameter space where the convective instabilities can arise, suggesting that some care may be needed in setting up the experimental conditions for their realization. Our calculations reveal, however, that this 'window' could be increased considerably if operating conditions are arranged so that ε is made larger, say by lowering the acidity. This is illustrated in Fig. 10a where we show the region of convective instability, labelled CU in the figure, in the ε–f parameter plane. (Here for $q = 0.002$, though the region is insensitive to the choice of q provided it is small.) The figure also shows the region where the system is absolutely unstable (AU). This corresponds to oscillatory responses in the batch system and gives a continuous propagating wave train in the present model. Outside these regions the system is stable for all flow rates. The effect of increasing ε (for given values of f and q) is to increase the critical flow rate $\phi_{\min}$ for the onset of DIFICI waves. This is illustrated in Fig. 10b, where we plot $\phi_{\min}$ against ε (for $f = 2.32$). Except for very small values of ε, $\phi_{\min}$ increases linearly with ε. In general, $\phi_{\min}$ increases with increasing f and ε within the convective instability boundary. This suggests that operating the reactor under less 'excitable' conditions could require a sufficiently large critical flow rate for DIFICI waves that may be observed experimentally.

The general conclusions from the above are that the results from our model are in, at least, qualitative agreement with the experiments and can play a useful role in predicting possible behaviour. However, there is one feature of the model that is different to what is observed. Namely, the numerical simulations show each wave in the wave train starting progressively further downstream. This is not seen in the experiments, where the propagating wave patterns appear to fill the whole length of the reactor throughout a particular run. There could be several reasons for this. The numerical computations are for a relatively short reactor of length approximately 14 cm (using eqn. (19)) as compared to the 30 cm used and so these represent only the first part of the reactor. Perhaps more importantly, only a single perturbation was applied as the initial condition in the numerical simulations, whereas in the experiments there will be slight perturbations to the operating conditions (*e.g.* inflow rates) throughout. Previous general work on convective instabilities[24] and for chemical systems[27] shows that convective instabilities can considerably enhance any slight time-dependent inlet perturbations, thus producing a continuous generation of waves. These then appear along the whole length of the reactor for that run.

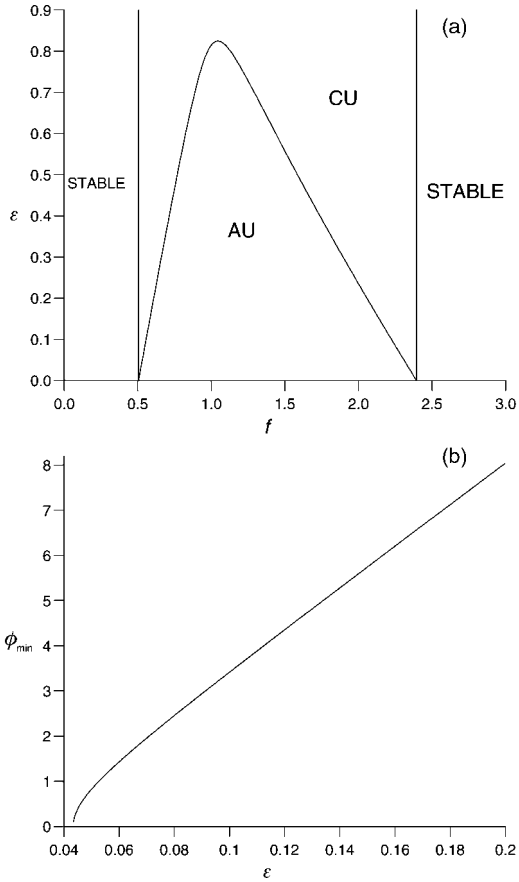

Fig. 10 (a) A plot in the ε–f parameter plane showing the region of convective instability (CU) and absolute instability (AU) (for $q = 0.002$). (b) $\phi_{\min}$ plotted against ε for $f = 2.32$, $q = 0.002$.

Acknowledgements

This work was supported by the British Council and the Hungarian Scholarship Board (Ministry of Education) under the Joint Academic Research Programme (project number 010), by the ESF Scientific Programme REACTOR and by the Hungarian Research Grants OTKA T025375 and FKFP 0455/1997.

References

1 A. M. Turing, *Philos. Trans. R. Soc. London, Ser. B*, 1952, **237**, 37.
2 V. Castets, E. Dulos, J. Boissonade and P. DeKepper, *Phys. Rev. Lett.*, 1990, **64**, 2953.

3 Q. Ouyang and H. L. Swinney, *Nature*, 1991, **352**, 610.
4 I. Lengyel, S. Kádár and I. R. Epstein, *Science*, 1993, **259**, 493.
5 B. R. Johnson and S. K. Scott, *Chem. Soc. Rev*., 1996, **25**, 265.
6 A. B. Rovinsky and M. Menzinger, *Phys. Rev. Lett*., 1992, **69**, 1193.
7 A. B. Rovinsky and M. Menzinger, *Phys. Rev. Lett*., 1993, **70**, 778.
8 M. Menzinger and A. B. Rovinsky, in *Chemical Waves and Patterns*, ed. R. Kapral and K. Showalter, Kluwer, Dordrecht, 1995, pp. 365–397.
9 X.-G. Wu, S. Nakata, M. Menzinger and A. Rovinsky, *J. Phys. Chem*., 1996, **100**, 15810.
10 M. Sangalli and H.-C. Chang, *Phys. Rev. E*, 1994, **49**, 5207.
11 R. A. Satnoianu, J. H. Merkin and S. K. Scott, *Physica D*, 1998, **124**, 345.
12 R. A. Satnoianu, J. H. Merkin and S. K. Scott, *Chem. Eng. Sci*., 2000, **55**, 461.
13 R. A. Satnoianu, J. H. Merkin and S. K. Scott, *Dynam. Stabil. Syst*., 2000, **15**, 209.
14 D. Šnita, P. Hasal and J. H. Merkin, *Physica D*, 2000, **141**, 155.
15 M. Kaern and M. Menzinger, *Phys. Rev. E*, 1999, **60**, 3471.
16 A. N. Zaikin and A. M. Zhabotinsky, *Nature*, 1970, **225**, 535.
17 R. J. Field, E. Kőrös and R. M. Noyes, *J. Am. Chem. Soc*., 1972, **94**, 8649.
18 R. J. Field and R. M. Noyes, *J. Chem. Phys*., 1974, **60**, 1877.
19 S. K. Scott, *Chemical Chaos*, Clarendon Press, Oxford, 1991.
20 J. J. Tyson and P. C. Fife, *J. Chem. Phys*., 1980, **73**, 2224.
21 J. J. Tyson, in *Nonlinear Phenomena in Chemical Dynamics*, ed. C. Vidal and A. Pacault, Springer, Berlin, 1981, pp. 222–227.
22 J. D. Dockery, J. P. Keener and J. J. Tyson, *Physica D*, 1988, **30**, 177.
23 H. Jeffreys and B. S. Jeffreys, *Methods of Mathematical Physics*, Cambridge University Press, Cambridge, 1962.
24 R. J. Deissler, *J. Stat. Phys*., 1985, **40**, 371.
25 R. J. Deissler, *J. Stat. Phys*., 1989, **54**, 1459.
26 J. A. Leach, J. H. Merkin and S. K. Scott, *Proc. R. Soc. London, Ser. A*, 1993, **345**, 229.
27 R. A. Satnoianu, J. H. Merkin and S. K. Scott, *Dynam. Stabil. Syst*., 1999, **14**, 275.